Research Article Vol. 1, No. 8 / 15 Aug 2022 / Optics Continuum 1837

OPTICS CONTINUUM

Approach for faster signal processing in ϕ-OTDR systems based on the directional measurement of fiber slice interaction

MOHAMMADMASOUD ZABIHI* AND KATERINA KREBBER

Bundesanstalt für Materialforschung und -prüfung (BAM), Unter den Eichen 87, 12205 Berlin, Germany
*masoud.zabihi@bam.de

Abstract: Recently, fully distributed fiber sensors such as C-OTDR and ϕ-OTDR systems have drawn considerable attention from researchers. These sensors are ideal for industrial use because of their wide dynamic range, good spatial resolution, and high accuracy. However, for distributed acoustic sensors (DAS), the agility of sensor response, processing time, and data stacking have been significant challenges. These limitations are exacerbated in seismology applications for which we must record data for several hours or even several days. In this study, based on the interaction between scattering disks in a sensing fiber, we presented a new signal processing approach for heterodyne DAS systems. This approach can lead us to a direct measurement without the requirement of using or creating bulky functions in our computer interface. These measurements are easy to implement either in machine-level or high-level programming languages. We demonstrated that the speed of a DAS system can be increased while system parameters suffer only minor or no degradation. This processing idea provided us with a signal-to-noise ratio that was 1.5 dB higher than a conventional method; moreover, it increased the speed by ~40%.

1. Introduction

Distributed acoustic sensors (DAS) based on coherent optical time domain reflectometry (C-OTDR) and phase-sensitive optical time domain reflectometry (ϕ-OTDR) have drawn considerable attention from researchers as well as investments because of their accuracy, sensitivity, spatial resolution, and monitoring capabilities [1]. DAS have broad applications from seismology to structural monitoring, intrusion detection, threat prevention, and reservoir monitoring. Commonly, for coherent optical time-domain reflectometry systems, there are multiple known methods for signal demodulation [2]. Traditional value differentiation, edge detection, and wavelet packet decomposition are examples of the signal extraction process for DAS [3–5]. With the development of ϕ-OTDR systems we became capable to measure the frequency of the vibrations, as well as the location of them. But still in longer dynamic ranges, systems always require additional data processing; and sometimes we must sacrifice either sensing range or agility in our systems. Lin et al. [2] proposed a matrix matching method to improve data processing. However, this approach is primarily used in direct detection setups, which are uncommon in the industry. The approach of that research is based on computer architecture modifications rather than signal processing ideas. Based on correlation measurements [6], a method was proposed which the laser central frequency was changed and therefore the laser frequency drift was one of their major challenges. Furthermore, the non-linearity of changes can cause considerable inaccuracy. For multiple consecutive shots, the mathematical solution seemed to be ambiguous and incomplete; moreover, this would result in a significantly large data stack and low speed. Zhang et al. [7] proposed a frequency coding approach. Each probe pulse had two probe frequencies, and the reference arm had one modulator. Because of this setup, the local oscillator was not purely a sample of the laser source. This can reduce quality, and the optical path difference between these

#456421 https://doi.org/10.1364/OPTCON.456421
Journal © 2022 Received 17 Feb 2022; revised 20 Jun 2022; accepted 14 Jul 2022; published 15 Aug 2022

OPTICS CONTINUUM

two modulators can lead to additional fading noises. Marie et al. [8] proposed a two-layer pattern recognition algorithm. Their system first analyses the suspected perturbation areas; then, in the second stage, it estimates the model and extracts the power distribution features. Such systems require training and therefore may not be suitable for seismic applications or monitoring of reservoirs. Furthermore, the improvement in speed they achieved was small, and it was not worth sacrificing accuracy. A chirped pulse is used in Ref. [9] along with a an extraction algorithm. Although the entire idea is new, the influence of non-linearities is considerable. Furthermore, no information about the processing time or data volume was provided.

In this study, we present a novel approach to signal processing in C-OTDR and ϕ-OTDR systems that can be directly applied to the acquired data and is fast and ideal for real-time monitoring systems. Moreover, it is suitable for high-level programming languages, which are inherently slow and require multiple internal functions to be performed. This method has also no need for any artificial intelligence [10]. This makes our system cheaper and suitable for industrial purposes.

2. Mathematical fundamentals

Distributed acoustic sensors (DAS) are based on Rayleigh scattering. The use of COTDR techniques has the advantages of significantly low noise level, wide dynamic range, and high resolution. The coherency length can be significantly increased by implementing an appropriate laser source and benefiting from a suitable modulator [11]. A Φ-OTDR scheme, which is derived from OTDR but uses a highly coherent laser as the light source, is commonly used to realize Rayleigh backscattering (RBS) and the change of phase resulting from external perturbations. This technology has been extensively used in multiple applications such as structural health monitoring, intrusion detection, underwater acoustics, and seismic monitoring [12]. Figure 1 shows a heterodyne Φ-OTDR system.

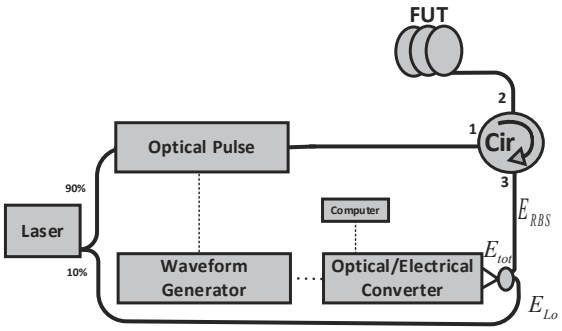

Fig. 1. Schematic of heterodyne ϕ-OTDR. System setup. Cir: Circulator; FUT: Fiber Under Test.

The amplitude and phase of scattered light are unique to each location along the fiber. To have the information of the backscattered signal, first we should attempt to independently obtain the electrical field of each cross-section (Fig. 2). It is also useful when we want to see the phase changes between to selected areas.

Each scattering disc consists of numerous scattering points which may have been caused by impurities or other mechanical reasons. Each scattering point emits the light in a random direction. However, the scattering phase of each point is constant for a given probe light. The scattering points that would backscatter light with angles smaller than the critical angles could be omitted. The backscattered signal $\Delta\overrightarrow{\varepsilon_b}(z)$ received at the fiber input from an arbitrary disc

OPTICS CONTINUUM

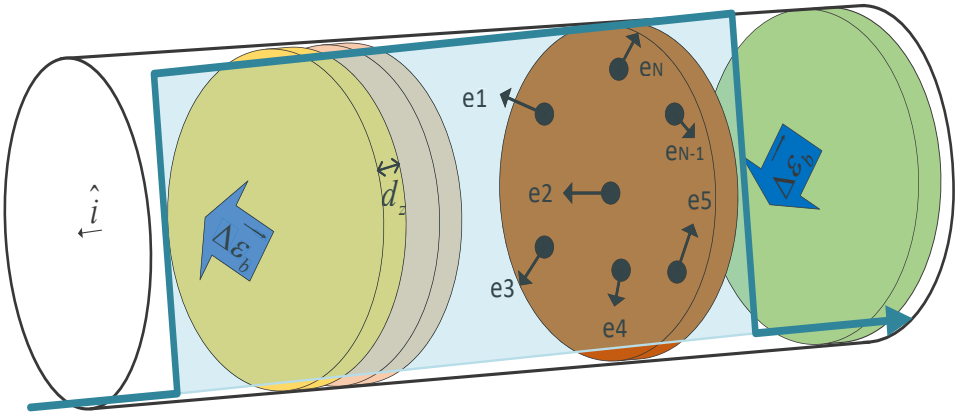

Fig. 2. Cross-section overview of an electrical field in sensing fiber.

located in z is [13]

$$\Delta\overrightarrow{\varepsilon_b}(z) = \frac{f_s(\widehat{O},\widehat{i})e^{(jkz)}}{z} \tag{1}$$

where $f_s(\widehat{O},\widehat{i})$ is the scattering amplitude, $\widehat{i}$ is direction of backscattering light, and k is the wavenumber. Based on Ref. [13],

$$|f_s(\widehat{O},\widehat{i})|^2 = \sigma(\widehat{O},\widehat{i})V \tag{2}$$

$\sigma(\widehat{O},\widehat{i})$ is the differential scattering disc per unit of volume and V is the volume of the scattering disc. Then, we can rewrite Eq. (1) as:

$$\Delta\overrightarrow{\varepsilon_b}(z) = \pm\frac{\sqrt{\sigma(\widehat{O},\widehat{i})V}e^{(jkz)}}{z} \tag{3}$$

Because the probe pulse stream is engaged with the negative values of the electric field, we only consider the positive one, which is backward and subject to Rayleigh backscattering. We can expand Eq. (3) by knowing:

$$\sigma(\widehat{O},\widehat{i}) = 2\pi k^4 \mathrm{Sin}^2(\chi)S_n(k_s) \tag{4}$$

where $S_n(k_s)$ is the spectral density function of refractive index fluctuation, and χ is the angle between the polarization direction and backscattering direction. Therefore,

$$\Delta\overrightarrow{\varepsilon_b}(z) = \frac{k^2\mathrm{Sin}(\chi)\sqrt{2\pi S_n(k_s)V}e^{(jkz)}}{z} \tag{5}$$

Using a polarization-controlled circulator will help us simplify this equation by ignoring the $\mathrm{Sin}(\chi)$ term.

To measure the total electrical field of RBS traces, we must apply the directional growth in the electric field of each disc to its neighbours. If we only have two disks, we have

$$\overrightarrow{\varepsilon}_{z\sim z+\Delta z} = (|\Delta\overrightarrow{\varepsilon_b}(z)||\Delta\overrightarrow{\varepsilon_b}(z+\Delta z)|\mathrm{Cos}\psi)\widehat{i} \tag{6}$$

where Ψ is the angle between these two electric fields and $\widehat{i}$ is the unit vector in the cylindrical system, which is considered an electrical field in the direction of the probe pulse. By putting

OPTICS CONTINUUM

Eq. (5) in Eq. (6) we achieve:

$$\overrightarrow{\varepsilon}_{z\sim z+dz} = (2\pi e^{2k} k^4 S_n(k_s) V \frac{e^{j(2z+dz)}}{z^2} \mathrm{Cos}\psi)\widehat{i} \tag{7}$$

The probe pulse affects a limited number of scattering disks based on its width (Fig. 2). Thus, $\overrightarrow{\varepsilon}_{z\sim z+dz}$ can be measured for a range equal to pulse width (PW).

$$PW = m \times dz \tag{8}$$

$$\varepsilon_{PW} = \sum_{q=1}^{m} 2\pi e^{2k} k^4 S_n(k_s) V \frac{e^{j(2z+(q\times dz))}}{z^2} \mathrm{Cos}\psi \tag{9}$$

And the pulse itself sweeps the whole fiber range. Then with another integration over Eq. (9) we will have,

$$\varepsilon_b = \iint_{fut} 2\pi e^{2k} k^4 S_n(k_s) \frac{e^{j(2z+(m\times dz))}}{z^2} \mathrm{Cos}\psi d\psi dz \tag{10}$$

ε_b represents the intensity of the backscattering signal at any moment. The backscattered electric field, which is being shifted to $\Delta\omega$ by a modulator, can then be expressed as follows [14]:

$$E_{RBS}(t) = \varepsilon_b . e^{\{j[(\omega_0+\Delta\omega)t+\Phi(t)]\}} \tag{11}$$

where ω_0 and $\Delta\omega$ are the angular frequency of the laser source and the modulator upshifting frequency, respectively.$\Phi(t)$ represents the phase of backscattered signal.

Regardless of phase noise, the output electric field at the detector (Fig. 1) can be given by [14]

$$E_{tot}(t) = E_{LO} . e^{(j\omega_0 t)} + E_{RBS} \tag{12}$$

E_{LO} is the amplitude of the light emitting in the local oscillator. Then the photocurrent can be expressed as follows [1]

$$i_{BPD} = R_d\{E_{LO}^2 + {\varepsilon_b}^2 + 2E_{LO}\varepsilon_b e^{j(\Delta\omega t+\Phi(t))}\} \tag{13}$$

R_d is the detector responsivity. By removing the DC part, the following simplified signal is obtained [15]:

$$i_{BPD}(t) = R_d\{2E_{LO}\varepsilon_b e^{j(\Delta\omega t+\Phi(t))}\} \tag{14}$$

$$i_{BPD}(t) = 4R_d\pi k^4 S_n(k_s) E_{LO} e^{j(\Delta\omega t+\Phi(t))+2k} \iint_{fut} \frac{e^{j(2z+(m\times dz))}}{z^2} \mathrm{Cos}\psi d\psi dz \tag{15}$$

Except $e^{j(\Delta\omega t+\Phi(t))+2k}$, other variables in Eq. (15) are known to us. Therefore, we can shape Eq. (16) and extract $\Phi(t)$ as follows,

$$e^{j(\Delta\omega t+\Phi(t))+2k} = \frac{i_{BPD}(t)}{4R_d\pi k^4 S_n(k_s) E_{LO} \iint_{fut} \frac{e^{j(2z+(m\times dz))}}{z^2} \mathrm{Cos}\psi d\psi dz} \tag{16}$$

We will then by applying Eq. (16) have a 1D dataset during each repetition period of the pulse. When we maintain a recording over time, we will have a data matrix. For having a numerical

OPTICS CONTINUUM

realization of the proposed method, we name this initial data matrix as the Intensity matrix.

$$Intensity\_Matrix = \begin{bmatrix} \alpha_{0,0} & . & . & \alpha_{0,i} & . & . & . & . & \alpha_{0,c} \\ . & . & . & . & . & . & . & . & . \\ . & . & . & . & . & . & . & . & . \\ \alpha_{r,0} & . & . & \alpha_{r,i} & . & . & . & . & a_{r,c} \end{bmatrix}_{r+1,c+1} \tag{17}$$

By applying Eq. (16) on the intensity matrix, we can get a new matrix calling Gamma matrix. The numerical realization of Gamma matrix is as follow,

$$Gamma\_Matrix = \begin{bmatrix} \left(\sum_{i=0}^{FW-1} \alpha_{0,i}^2\right) + \left(2\lambda \times \sum_{i=0}^{FW-2} \sum_{n=1}^{FW-1-i} \alpha_{0,i}\alpha_{0,i+n}\mathrm{Cos}(nR)\right) & . & \left(\sum_{i=1}^{FW} \alpha_{0,i}^2\right) + \left(2\lambda \times \sum_{i=1}^{FW-1} \sum_{n=1}^{FW-i} \alpha_{0,i}\alpha_{0,i+n}\mathrm{Cos}(nR)\right) & . & . & . \\ . & & . & & & \\ . & & . & & & \\ \left(\sum_{i=0}^{FW-1} \alpha_{p,i}^2\right) + \left(2\lambda \times \sum_{i=0}^{FW-2} \sum_{n=1}^{FW-1-i} \alpha_{p,i}\alpha_{p,i+n}\mathrm{Cos}(nR)\right) & . & \left(\sum_{i=1}^{FW} \alpha_{p,i}^2\right) + \left(2\lambda \times \sum_{i=1}^{FW-1} \sum_{n=1}^{FW-i} \alpha_{p,i}\alpha_{p,i+n}\mathrm{Cos}(nR)\right) & . & . & . \end{bmatrix}_{r+1,c-FW+1} \tag{18}$$

where:

$$\lambda = \frac{\ln(4R_d\pi k^4 S_n(k_s,t))}{2k} \tag{19}$$

$$FW = PulseWidth \times SamplingRate \tag{20}$$

$$R = \frac{2\pi \times IF}{SamplingRate} \tag{21}$$

Each row on the Gamma matrix is a single shot, processed by the Eq. (16), and each column corresponds a location on the fiber under test (Fig. 3). Next, similar to conventional methods [1]; we use a differential method between two distinct points on all shots in our desired time window, for vibration reconstruction. We consider two regions, such as A and B, to compare phase differences between backscattered light between them [12]. Regardless of fiber loss, the phase difference from A and B (Fig. 3) at $t = \tau_1$ and $t = \tau_2$ is as follows:

$$\Delta\Phi_{A\sim B} = \sum_{i=0}^{C+1} (\Phi_{t=\tau_1+(i\times R_P)} - \Phi_{t=\tau_2+(i\times R_P)}) \tag{22}$$

where $c + 1$ is the number of shots per the time window and R_P is the repetition period of the probe pulse. [12]. By measuring amplitude and phase with this technique, we can reconstruct the incoming vibration faster than conventional approaches.

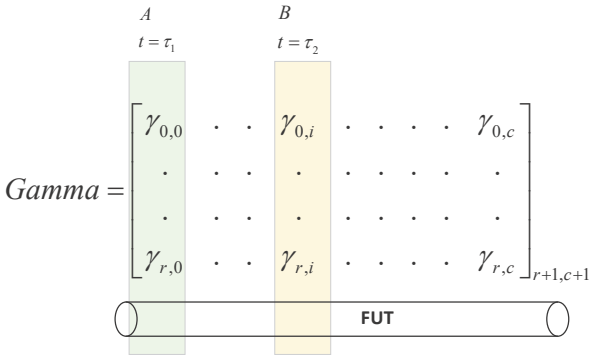

Fig. 3. The Schematic of Gamma matrix. Coloured bars are the arbitrary columns we can pick for phase extraction. Each column represents a location on FUT.

OPTICS CONTINUUM

Figure 4 shows the comparison between conventional method and the proposed Gamma matrix measurement. We can speed up the system by performing suggested method and avoid time consuming measurements by high level programming languages. The location and amplitude of vibration can be obtained directly from Eq. (18) and the phase of vibration comes from Eq. (22).

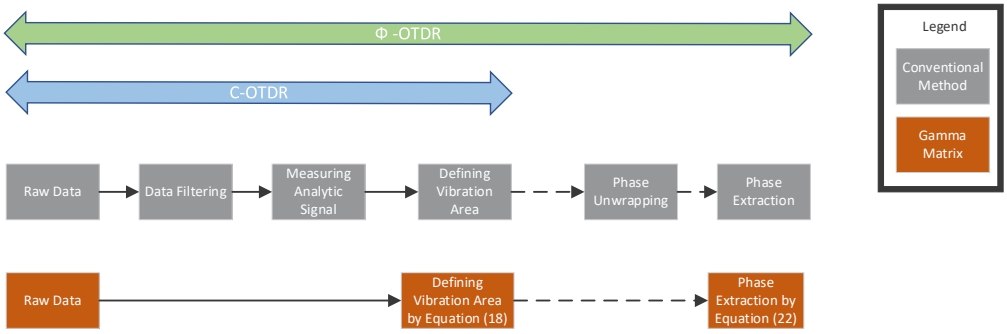

Fig. 4. Schematic comparison between conventional processing and Gamma matrix processing.

3. Experimental results

We used this method within two different tests, a laboratory test with high frequency event (Piezoelectric actuator) and low frequency event (walking event) and a field test in street and over an actual telecommunication cable, perturbing with hammer hits.

We created a heterodyne ϕ-OTDR setup as shown in Fig. 5. The output of a CW laser with frequency ω_0 (1550 nm, RIO ORION laser module) is split in a local oscillator and sensing light. In the first experiment, an acousto-optic modulator creates a probe pulse and shifts its frequency by 150 MHz. This pulse has a width of 100 ns with a repetition rate of 1 kHz. This value of repetition rate is quiet enough for reconstruction of both Piezoelectric actuation and walking event. The probe pulse is then launched into the FUT through a circulator after amplification in an EDFA. The first piece of fiber is 5000 m, followed by a 15 m cylindrical PZT actuator, which is stimulated with a sinusoidal wave of 60 Hz. Then, a 200 m fiber is located at the far end of the FUT.

The RBS returning from the FUT at frequency $\omega_0 + \Delta\omega$ is combined with the OLO (Eq. (12)) to produce the intermediate frequency. The optical signal is then converted to an electrical signal by a balanced photodetector having a bandwidth of 200 MHz. The data are captured using an acquisition card with a sampling rate of 500 MHz.

Figure 6 shows the results obtained from the first experiment with the gamma matrix method and output of a conventional demodulation system. As per the Python code results, for each independent measurement on the same device, the conventional measurement lasts almost twice more than gamma matrix measurement. Although the gamma matrix result is somewhat spiky, it provided us with a higher amplitude at the vibration location. It has a higher amplitude and better SNR, particularly at the beginning of the recording ($t = 0$), which is promising for applications which need early-stage detection. The location of vibration is shown in Fig. 7. This normalized 2D plot is more commonly used for long-range recordings and seismology. The blue boxes show that the gamma matrix method detected physical harmonics in neighboring areas even better and could be a good solution for micro bending and slow earth crust movements. Figure 8 shows a comparison between SNR achieved using the conventional method and gamma matrix. As we compared the peak value with the noise mean level in SNR calculation, both methods achieved almost the same values (22 dB).

OPTICS CONTINUUM

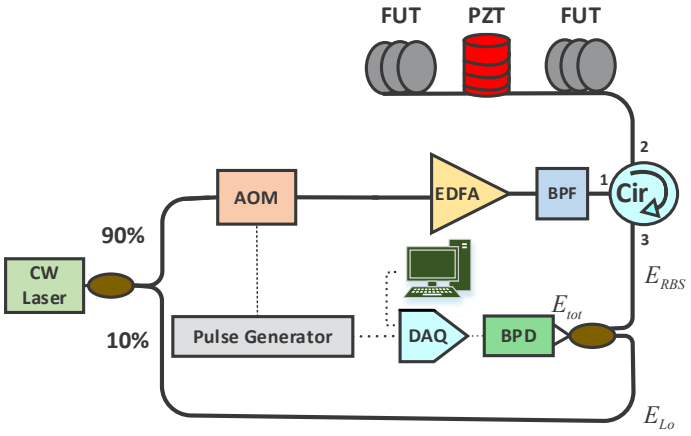

Fig. 5. Schematic of heterodyne ϕ-OTDR. System setup. CW Laser: Continuous Wave Laser; AOM: Acousto- Optical Modulator; EDFA: Er-Doped Fiber Amplifier; BPF: Bandpass Filter; Cir: Circulator; FUT: Fiber Under Test; PZT: Piezo-electric Transducer; BPD: Balanced Photo Detector; DAQ: Data Acquisition Card.

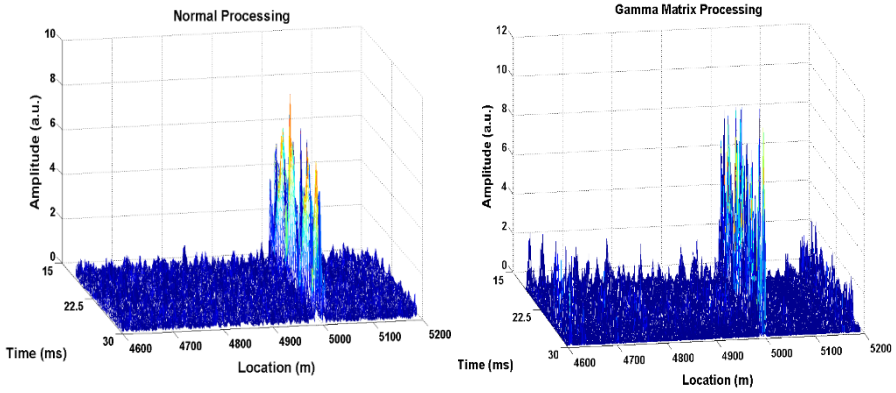

Fig. 6. 3D Reconstruction of the external perturbation by conventional method and Gamma matrix.

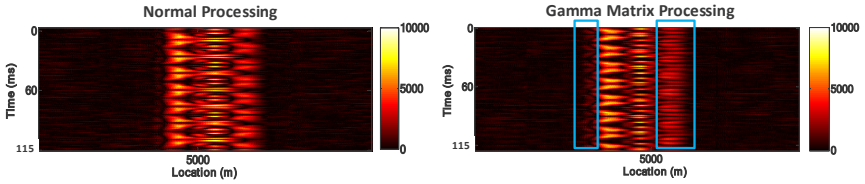

Fig. 7. 2D view comparison of the vibration area obtained by conventional measurement and Gamma matrix.

OPTICS CONTINUUM

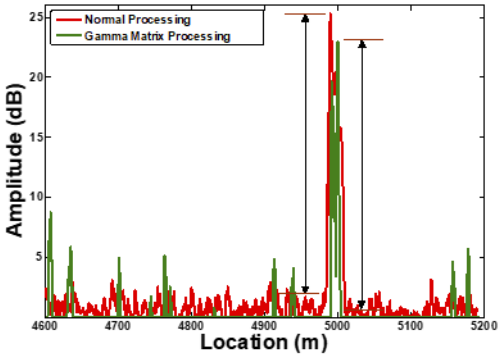

Fig. 8. SNR comparison in recording of 2 min.

For decapsulation of phase information, we required a few additional steps; however, these steps were made considerably faster and shorter by Eqs. (16)–(17). Rather than developing an entire demodulation matrix in other methods, we can extract the phase by shaping only two smaller blocks at a time. These two blocks represent two sides of the gauge [16]. As Fig. 3 shows, these two imaginary blocks are A and B. We can shape Gamma matrix and examine the vibration area and shape the two-phase extraction blocks by obtaining the initial data right after DAQ. Based on Eq. (10) we can directly obtain $\overrightarrow{\varepsilon_b}(A|_{t=\tau_1}) - \overrightarrow{\varepsilon_b}(B|_{t=\tau_2})$, then the electrical current and finally place it in Eq. (16). This will yield us phase changes between phase blocks in the gamma matrix.

The vibration at 60 Hz was successfully obtained using both methods (Fig. 9). The gamma matrix method not only showed the external perturbation but also revealed the physical odd harmonics (3^{rd} and 5^{th}) of the vibration event as explained for Fig. 7.

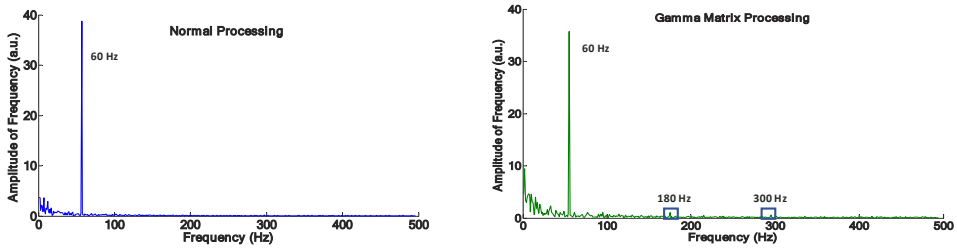

Fig. 9. Frequency content of the vibration obtained using these two methods

Then, the effectiveness of gamma matrix for low-frequency events was tested. A 12-m-shielded fiber was attached to the FUT end and laid on the ground. Then, a person walked back and forth five times close to this piece of fiber. We maintained the PZT in the system for validating the results. The PZT perturbation and walking events are shown in Fig. 10.

As it mentioned before, low-frequency events require long-term recording; thus, data processing consumes many hardware resources, e.g., in passive seismology applications, recording time is between several hours and days. This huge data would require significantly lengthy and huge processing. However, the 30s walking event in Fig. 10 was processed with a normal computer and using Gamma matrix only in 2 minutes.

The second experiment was performed on a dark fiber from an actual telecommunication cable under the street. In this case, environment was very noisy and the cable under the ground could be loose in many parts. Low frequency noises in the street and the depth of the trench (1.5m)

OPTICS CONTINUUM

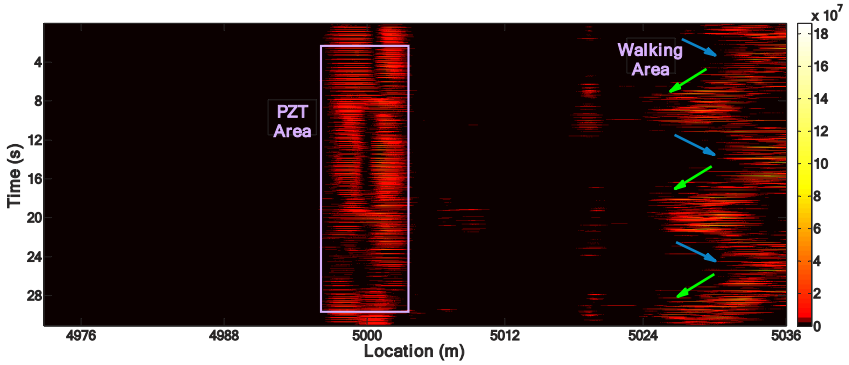

Fig. 10. Low-frequency event reconstruction with Gamma matrix

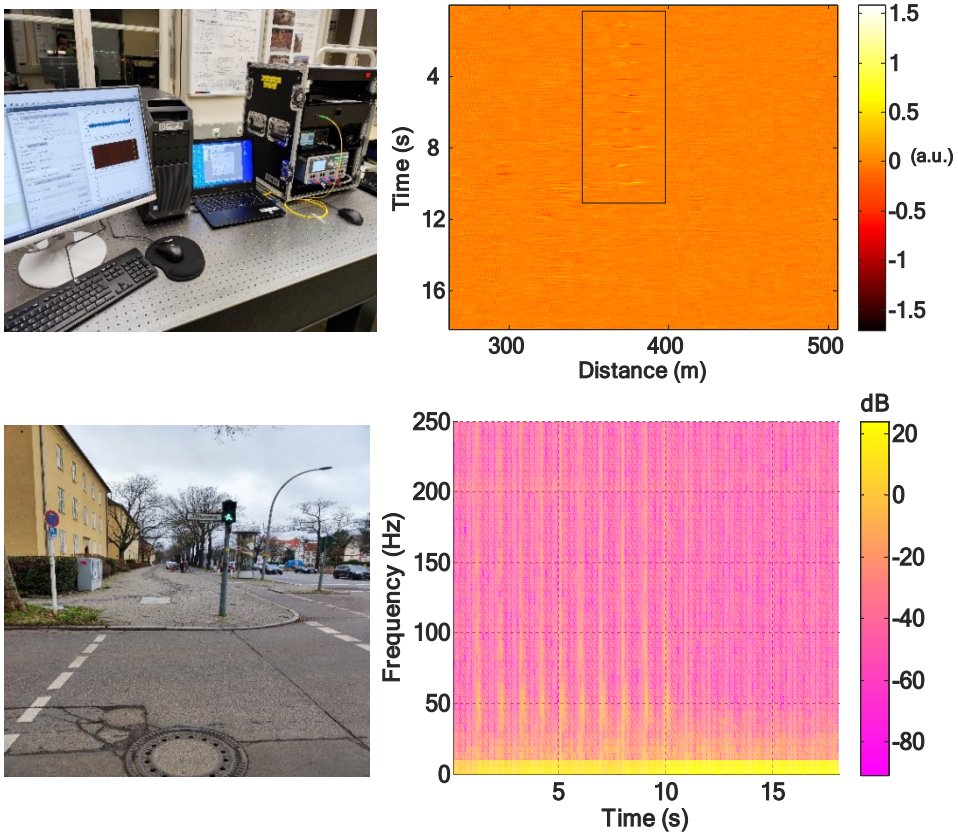

Fig. 11. 10 hammer hit events in on a buried telecommunication cable. The left side pictures show the system itself and the area the test was performed.

OPTICS CONTINUUM

could be limiting factors for any measurement system. This time we performed the test with 10 soft hammer hits and the pulse repetition rate was 500Hz.Then, it was expected the hammer hits being seen in the whole frequency range. Figure 11. Shows the system using Gamma matrix can detect the perturbation clear and very fast. Although it was a noisy location, but the upper-right figure is acceptably noise free and shows the place and the time of hammer strikes clearly. The lower-right figure illustrates the frequency of hits evolving in time. As it is expected, the frequency of hits is expanded withing the whole 250Hz bandwidth.

4. Summary

In this study, a signal processing approach for heterodyne ϕ-OTDR and C-OTDR systems that can obtain external perturbation and its frequency content in a faster way is proposed. We can detect vibrations with the same or better SNR using this processing approach, only with a single step and fast calculation. Figure 12 shows the comparison of the normalized measurement time for the gamma matrix method and the conventional method throughout the three experiments. The speed of processing using a gamma matrix is ~35%–50% faster compared to a conventional method in high frequency test (PZT), low frequency test (walking) and street monitoring test. The processing speed in low frequency test is normally a bit lower than the similar high frequency one, since we must use higher number of time frames. Also, in street test we have higher speed because we can select wider gauges.

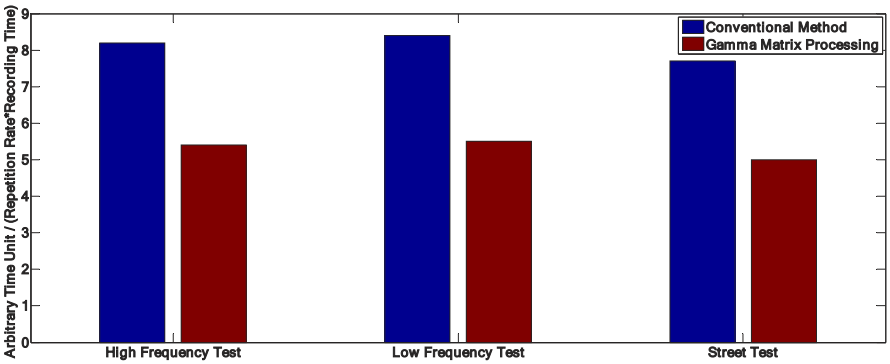

Fig. 12. Comparison between the speed of a conventional processing with Gamma matrix processing

This approach is easy to implement with machine -level programming languages and does not require lengthy processing for bandpass filtering and analytical signal extraction. This is particularly useful for long-term data recordings for seismic applications, and it helps in the implementation of a real-time interrogation system. Depending on the design and applications, Gamma matrix processing enhanced the speed between 35% and 50% for these experiments.

Funding. Federal Ministry for Economic Affairs and Climate Action (FKZ: 03EE4009B).

Acknowledgments. This research was carried out in the framework of the research project "Distributed fiber optic strain sensing along existing telecommunication networks for efficient seismic exploration and monitoring of geothermal reservoirs" (project acronym SENSE). It was supported by the Federal Ministry for Economic Affairs and Climate Action, FKZ: 03EE4009B. The authors thank for the financial support and all the partners of the project consortium for helpful discussions. We also thank Sebastian Chruscicki and Sven Münzenberger from BAM for their technical supports.

Disclosures. The authors declare no conflicts of interest.

Data availability. Data underlying the results presented in this paper are not publicly available at this time but may be obtained from the authors upon reasonable request.

OPTICS CONTINUUM

References

1. A. H. Hartog, *An introduction to distributed optical fibre sensors* (CRC Press, 2017).
2. X. Liu, Y. Wang, R. Wu, D. Wang, Q. Bai, and B. Jin, "Real-Time phase-sensitive OTDR based on data matrix matching method," Sensors **18**(6), 1883 (2018).
3. J. Park and H. F. Taylor, "Fiber optic intrusion sensor using coherent optical time domain reflectometer," Jpn. J. Appl. Phys. **42**(6A), 3481–3482 (2003).
4. T. Zhu, X. Xiao, Q. He, and D. Diao, "Enhancement of SNR and Spatial Resolution in φ-OTDR System by Using Two-Dimensional Edge Detection Method," J. Lightwave Technol. **31**(17), 2851–2856 (2013).
5. Q. Li, C. Zhang, and C. Li, "Fiber-optic distributed sensor based on phase-sensitive OTDR and wavelet packet transform for multiple disturbances location," Optik **125**(24), 7235–7238 (2014).
6. Y. Zhi, S. Pengxiang, and L. Yongqian, "Research on COTDR for measuring distributed temperature and strain," in *2011 Second International Conference on Mechanic Automation and Control Engineering* (IEEE2011), pp. 590–593.
7. X. Zhang, Y. Song, and L. Lu, "Time division multiplexing optical time domain reflectometry based on dual frequency probe," IEEE Photonics Technol. Lett. **24**(22), 2005–2008 (2012).
8. T. F. B. Marie, D. Han, and B. An, "Pattern recognition algorithm and software design of an optical fiber vibration signal based on Φ-optical time-domain reflectometry," Appl. Opt. **58**(31), 8423–8432 (2019).
9. J. Xiong, Z. Wang, Y. Wu, and Y. Rao, "Single-shot COTDR using sub-chirped-pulse extraction algorithm for distributed strain sensing," J. Lightwave Technol. **38**(7), 2028–2036 (2020).
10. S. Liehr, L. A. Jäger, C. Karapanagiotis, S. Münzenberger, and S. Kowarik, "Real-time dynamic strain sensing in optical fibers using artificial neural networks," Opt. Express **27**(5), 7405–7425 (2019).
11. Y. Bai and Q. Bai, *Subsea pipeline integrity and risk management* (Gulf Professional Publishing, 2014).
12. M. Zabihi, Y. Chen, T. Zhou, J. Liu, Y. Shan, Z. Meng, F. Wang, Y. Zhang, X. Zhang, and M. Chen, "Continuous fading suppression method for Φ-OTDR systems using optimum tracking over multiple probe frequencies," J. Lightwave Technol. **37**(14), 3602–3610 (2019).
13. M. Nakazawa, "Rayleigh backscattering theory for single-mode optical fibers," J. Opt. Soc. Am. **73**(9), 1175–1180 (1983).
14. M. Zabihi, X. Chen, T. Zhou, J. Liu, F. Wang, Y. Zhang, and X. Zhang, "Compensation of optical path difference in heterodyne Φ-OTDR systems and SNR enhancement by generating multiple beat signals," Opt. Express **27**(20), 27488–27499 (2019).
15. A. Masoudi, M. Belal, and T. Newson, "A distributed optical fibre dynamic strain sensor based on phase-OTDR," Meas. Sci. Technol. **24**(8), 085204 (2013).
16. T. Dean, T. Cuny, and A. H. Hartog, "The effect of gauge length on axially incident P-waves measured using fibre optic distributed vibration sensing," Geophysical Prospecting **65**(1), 184–193 (2017).